ACS APPLIED MATERIALS & INTERFACES

Research Article

www.acsami.org

Effect of Lithiation Potential and Cycling on Chemical and Morphological Evolution of Si Thin Film Electrode Studied by ToF-SIMS

Catarina Pereira-Nabais,[†] Jolanta Światowska,*[,†] Michel Rosso,[‡] François Ozanam,[‡] Antoine Seyeux,[†] Aurélien Gohier,[§] Pierre Tran-Van,[§] Michel Cassir,[†] and Philippe Marcus[†]

[†]Institut de Recherche de Chimie Paris, CNRS—Chimie ParisTech, 11 rue Pierre et Marie Curie, 75005 Paris, France

[‡]Laboratoire de Physique de la Matière Condensée, CNRS (UMR 7643), École Polytechnique, 91128 Palaiseau, France

[§] Renault, Electric Storage System Division, 1 avenue du Golf, 78288 Guyancourt, France

ABSTRACT: Si thin films obtained by plasma enhanced chemical vapor deposition (PECVD) were used to investigate chemical and morphological modifications induced by lithiation potential and cycling. These modifications were thoughtfully analyzed by time-of-flight secondary ion mass spectrometry (ToF-SIMS) depth profiling, which allows to distinguish the surface and bulk processes related to the formation of the solid electrolyte interphase (SEI) layer, and Li−Si alloying, respectively. The main results are a volume expansion/shrinkage and a dynamic behavior of the SEI layer during the single lithiation/delithiation process and multicycling. Trapping of lithium and other ions corresponding to products of electrolyte decomposition are the major reasons of electrode modifications. It is shown that the SEI layer contributes to 60% of the total volume variation of Si electrodes (100 nm). The apparent diffusion coefficient of lithium (D_{Li}) calculated from the Fick's second law directly from Li-ion ToF-SIMS profiles is of the order of ~5.9×10^{-15} $cm^2.s^{-1}$. This quite low value can be explained by Li trapping in the bulk of electrode material, at the interfaces, continuous growth of the SEI layer and increase of SiO_2 quantity. These modifications can result in limitation the ionic transport of Li.

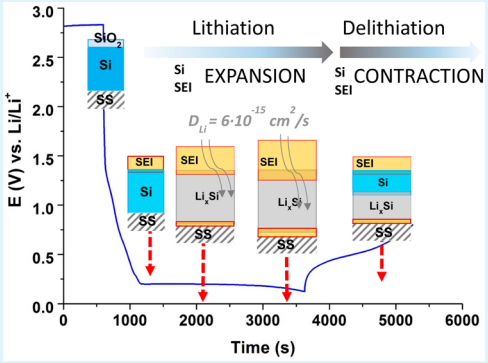

KEYWORDS: *Si thin film electrode, SEI layer, ToF-SIMS, volume expansion/shrinkage, Li trapping, diffusion*

1. INTRODUCTION

Very high charge capacity (3579 mAh/g) of Si negative electrode in Li-ion batteries is related to the formation of Li-rich alloys. However, the lithium alloying/dealloying reaction leads to huge volume variation and high mechanical stresses that are responsible for electrode cracking and crumbling which can trigger poor cycling ability.[1−3] It has been reported recently that a poor cyclability of Si electrodes was associated with lithium segregation[4,5] and induced stresses[6] at the electrode/current collector interface. The volume variations of Si electrode and resulting electrode cracking entail a continuous growth of solid electrolyte interphase (SEI) layer on the newly exposed surface of Si electrode.[7,8] Thus, taking into consideration these modifications, the formation of the SEI layer is not only limited to the first lithiation/delithiation cycle but it continues in the following cycles. It should be also emphasized that the morphology and composition of the SEI layer strongly depend on the electrolyte composition[9−15] and state of lithiation.[16−19]

In this Research Article, the composition of the SEI layer, and the chemical and the morphological modifications of the Si (a-Si:H) thin film electrode were studied as a function of lithiation potential and number of cycles by means of time-of-flight secondary ion mass spectrometry (ToF-SIMS) depth profiles. ToF-SIMS is a surface sensitive technique allowing for local ions detection (i.e., lithium ions and species characteristic of the products of electrolyte decomposition and analyzed sample) with a high sensitivity and a very high in-depth resolution (~1 nm).[7,8] Moreover, changes in the in-depth ions intensities and modifications in time of sputtering induced either by lithiation potential or cycling allow an easy discrimination between SEI layer zone, Si thin film electrode zone and stainless steel (SS) current collector zone. The application of the Si model thin film electrode having enlarged surface-to-volume ratio, provides clear and more comprehensible insight into the electrode/electrolyte interface reactions without complications from current percolators or binding agents[8] that are used in bulk composite electrode materials. This allows us to study intrinsic electrochemical and interfacial processes occurring on the surface of electrode materials. ToF-SIMS depth profile is also used for the direct calculation of the apparent diffusion coefficient of Li ions (D_{Li}) in 100 nm Si films using the semi-infinite integration of Fick's second law for one-dimensional diffusion.

Received: May 13, 2014
Accepted: July 24, 2014
Published: July 24, 2014

2. EXPERIMENTAL CONDITIONS

Si thin film electrodes (hydrogenated amorphous silicon: a-Si:H) with two different thicknesses, 30 and 100 nm, were prepared by plasma assisted chemical vapor deposition (PECVD) on stainless steel (SS) substrate (AISI321, Goodfellow). Details concerning the sample preparation by means of PECVD were given in a previous paper.[8] For simplicity, the a-Si:H thin film electrodes will be denoted "Si thin film electrodes".

Electrochemical cycling of the Si thin film electrode with thicknesses of 30 and 100 nm was performed in a two-electrode half-cell (Teflon Swagelok type) (as described in a previous paper[8]). A paper filter was used as separator and propylene carbonate (PC, purity >99.7%, 20 ppm of H_2O, Sigma-Aldrich) containing 1 M $LiClO_4$ (purity >99.99%, battery grade, Sigma-Aldrich) was used as electrolyte. The concentration of water in the electrolyte was lower than 30 ppm, as controlled by a Karl Fischer coulometer. A lithium foil (99.9% purity, Alfa Aesar) was used as both counter and reference electrodes. Cells were assembled in an Ar-filled glovebox ($O_2 \approx 1$ ppm; $H_2O < 3$ ppm). The cells were cycled galvanostatically between 0.125 and 2 V vs Li/Li^+ at a charge/discharge rate of C/1 (full charge or discharge in 1 h), corresponding to 25 and 84 $\mu A/cm^2$ for 30 and 100 nm film thicknesses, respectively, considering material density equal to 2.33 g/cm^3 and a maximum capacity of 3600 mAh/g. Potentiometric curves were acquired by a VMP3 Biologic multichannel potentiostat/galvanostat equipped with EC-Lab software for data acquisition. After cycling, the cells were opened in the glovebox and the cycled Si films were rinsed with dimethyl carbonate (DMC, ≥ 99% purity, Sigma-Aldrich) and dried under argon flow before ToF-SIMS analysis.

An IONTOF ToF-SIMS 5 spectrometer (time-of-flight secondary ion mass spectrometry) to which the glovebox is directly coupled, was used in the dual beam analysis mode to collect negative-ion depth profiles for pristine and cycled Si films. For sputtering a 2 keV Cs^+ beam with a 100 nA current was rastered on a 300 × 300 μm^2 area, while for analysis a 25 keV Bi^+ beam with a 1.2 pA current in a 100 × 100 μm^2 area centered at the bottom of the crater was used. Both beams hit the target at an angle of 45°. The spectrometer was run at an operating pressure of 10^{-9} mbar. Data acquisition and processing were done using the Ion-Spec software.

3. RESULTS AND DISCUSSION

3.1. Electrochemical Properties. *3.1.1. Galvanostatic Lithiation–Delithiation Process of Si Thin Film Electrode.* Figure 1a shows the first cycle of lithiation/delithiation performed on a 100 nm Si film at a current density of 84 $\mu A/cm^2$ (i.e., C/1). In the first few hundreds of seconds, a steady decrease in the potential (marked as zone **a**, in Figure 1a), is attributed to SiO_2 reduction and SEI layer formation onto the Si surface. The second zone (marked as **b**, in Figure 1a) can be defined as a lithiation plateau, and the third zone (marked as **c**, in Figure 1a) as a delithiation one.

The galvanostatic measurement was stopped at different states of lithiation and delithiation (marked from 1 to 5) and at each of them, the cell was left to relax until reaching a stable open circuit potential (OCP) with a variation less than 1 mV/h: at 200 mV before silicon lithiation plateau (point 1), at silicon half-lithiation plateau (point 2), at the end of lithiation at 125 mV (point 3), in the middle of delithiation at 500 mV (point 4), and in the end of delithiation at 800 mV (point 5).

The evolution of the OCP during the cell relaxation (at each point from 1 to 5) is marked by dashed red lines in Figure 1a.

At the first point of relaxation (point 1), a huge potential increase from 200 mV (lithiation cutoff potential E_{cutoff}) up to ~900 mV (E_{OCP}) versus Li/Li^+ can be observed, which may indicate a poor and unstable modification of Si bulk, mainly limited to the outermost part of the thin film electrode. The amount of lithium ions introduced into the bulk of the Si film

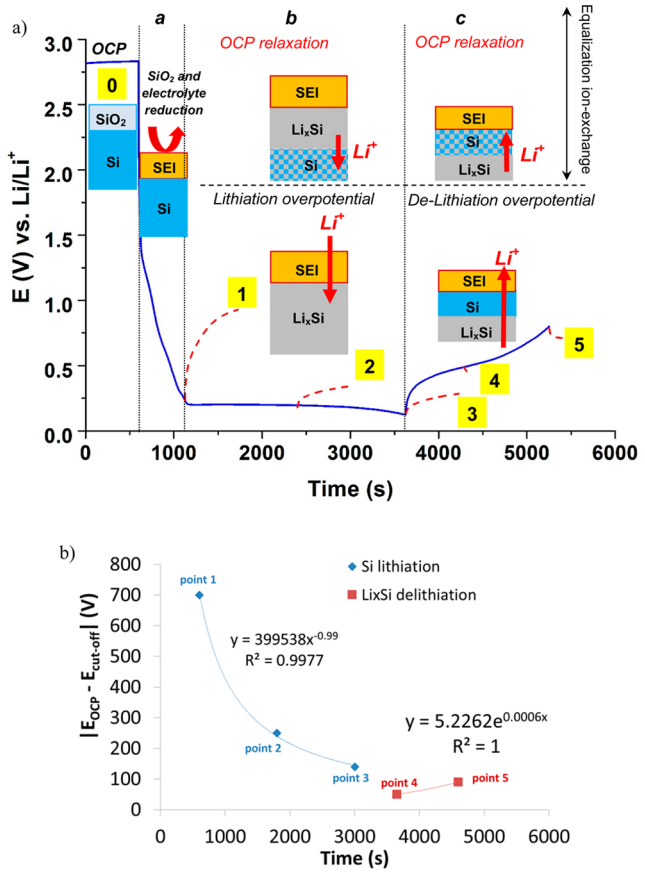

Figure 1. (a) Galvanostatic curve of the first cycle for 100 nm Si thin film (blue solid line). Red dashed lines show the E_{OCP} curves collected at 200 mV (point 1), 200 mV half lithiation plateau (point 2), 125 (point 3), 500 (point 4), and 800 mV (point 5). (b) E_{OCP} variation with time for lithiation and delithiation processes.

was gradually increased by decreasing the cutoff potential (point 2 and 3, Figure 1a). For these two points (2 and 3), a smaller potential increase (E_{OCP}) was observed in comparison with the first point: from 200 mV up to 450 mV and from 125 mV up to 265 mV, respectively (see red dashed lines in Figure 1a). Figure 1b shows the difference between the cutoff lithiation potential (E_{cutoff}) and the final OCP (E_{OCP}) as a function of time of lithiation. This difference between the lithiation potential (E_{cutoff}), and the final OCP (E_{OCP}) is diminished with the increase in the lithium content inside the Si bulk, showing an exponential dependence. A smaller deviation of the E_{OCP} from the E_{cutoff} can indicate more significant and stable modifications of the Si thin-film electrode related to formation of a stable Si–Li phase. Whereas, the surface processes occurring at the first lithiation potential (i.e., point 1) do not involve the bulk modifications like formation of stable Si–Li phases. The surface process might be a nonsteady-state process, with deposition of products related to reduction of electrolyte and formation of passive layer on the electrode surface. Thus, the weakly bonded to surface products of electrolyte decomposition containing lithium can be much easier detached from the surface and transferred back to the bulk electrolyte than the lithium forming the stable Si–Li phases.

Then, the a-Li_xSi:H film was progressively delithiated by applying a positive current and by controlling the cutoff oxidation potential (points 4 and 5 in Figure 1a). Similarly to lithiation process, at each point (4 and 5) the cell was relaxed

and the OCP was measured. In this case, a decrease in the E_{OCP} from 500 to 450 mV (point 4) and from 800 down to 710 mV (point 5) can be observed during delithiation (Figure 1a). Figure 1b shows a less significant difference between the final E_{OCP} and E_{cutoff} delithiation potential (red markers, points 4 and 5) than between the final E_{OCP} and the E_{cutoff} lithiation potential (blue markers, points 1−3). From the plot given in Figure 1b, it can be deduced that the difference between the cutoff potential (E_{cutoff}) (under current control) and the final E_{OCP} measured at each relaxation point is mainly due to the incomplete lithiation of the silicon matrix. As long as there are nonlithiated regions in the silicon matrix, lithium ions tend to diffuse toward lower concentration regions to reach an equilibrium state with a homogeneous distribution of lithium ions in the bulk of the electrode material. The schemes given in Figure 1a (zone b and c) illustrate lithium diffusion from rich (a-Li_xSi:H) to poor lithiated (a-Si:H) regions. It can also be observed that differences are less pronounced in the delithiation process. These results indicate that the distribution of lithium in the bulk electrode is more homogeneous during delithiation than during lithiation. The differences in lithium distribution can be also related to morphological modifications like expansion and contraction phenomena observed during lithiation and delithiation reactions, respectively. Diffusion concentration of lithium ions, ions related to products of electrolyte decomposition, and products of alloying reaction on the electrode surface and in the bulk electrode material as a function of lithiation potential and number of cycles were analyzed by ToF-SIMS in-depth profiling. The data will be presented in the following sections.

3.1.2. Capacity Retention of Si Thin Film Electrode. The cycling of the 30 nm-thick Si electrode shows a rather stable capacity in the range of 2500−2000 mAh/g (Figure 2a). The low columbic efficiency (Figure 2 a) during the first cycles can be related to the formation of SEI layer due to the reductive decomposition of electrolytes as discussed already in our previous paper.[8] During the first 20 cycles, an increase in the Columbic efficiency can be observed up to around 95%, which is stabilized in further cycles from 20 to 80, with a stable decrease observed during the last 20 cycles.

Figure 2b presents a capacity loss as a function of the cycle number for 30 and 100 nm Si film electrodes. A very high capacity loss can be observed for both thin film electrodes during the first few cycles. However, thinner films suffer from higher capacity loss during the first 25 cycles as shown in Figure 2b. Partly, this higher capacity loss for 30 nm thick silicon electrode can be related to the surface reactions occurring not only on the surface of Si-electrode but also on the stainless steel substrate (current collector), related to electrolyte reduction and/or to the conversion reactions of lithium with iron and chromium oxides from the stainless steel substrate.[20,21] The conversion reactions related to the formation of lithium oxide and metallic iron/chromium occur at a potential very close to that of electrolyte reduction.[21−23] The three times higher amount of electroactive material in the 100 nm-thick electrode with respect to the 30 nm-thick one, indicates, that all surface-like reactions which could occur on the thicker Si electrode are hidden by bulk reactions related to formation of a-Li_xSi:H alloys.

3.2. Chemical Modifications of Si Thin Film Electrodes Studied by ToF-SIMS Depth Profiling. *3.2.1. Influence of Lithiation State.* Tof-SIMS depth profiles (negative ions) were collected at different stages of lithiation and delithiation

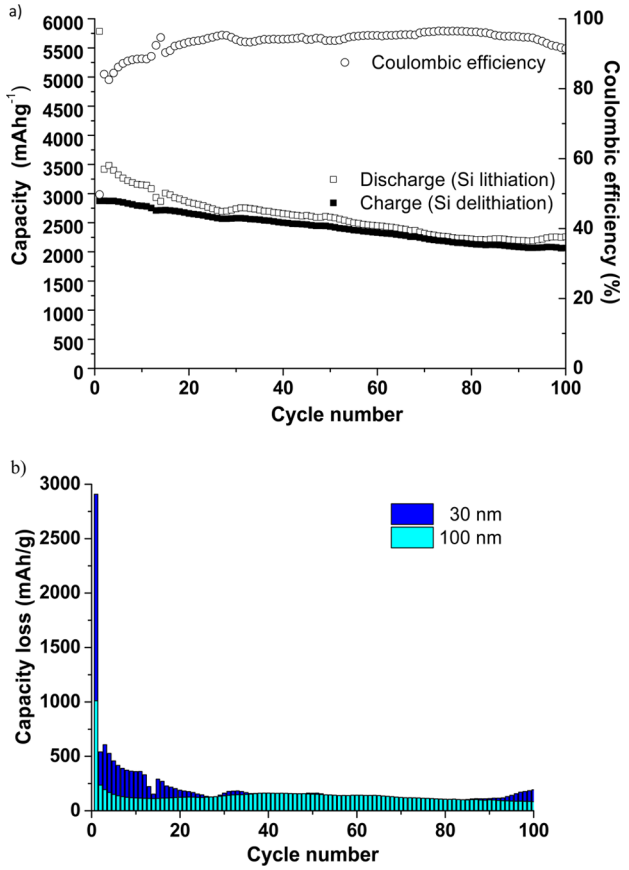

Figure 2. (a) Lithiation and delithiation capacity as a function of the number of cycles for 30 nm Si thin film electrode cycled in the potential range from 125 mV to 2 V vs Li/Li$^+$. (b) Capacity loss as a function of the number of cycles for the two Si film thickness (30 and 100 nm).

(analysis points from 0 to 5 are indicated in Figure 1a) of Si thin film electrode to investigate the following points: (1) volume and chemical changes produced at different lithiation states by collecting Si^-, SiH^-, and SiO_2^- ions, (2) formation of the SEI layer by acquiring Cl^-, CO_3^-, and Li^- ions, (3) formation of Li−Si alloys by registering $LiSi^-$ ions, and (4) presence and formation of pinholes into Si film by collecting signal characteristic of stainless steel current collector (SS substrate), as CrO^- ion.

Figures 3a-d shows ToF-SIMS depth profiles of pristine 100 nm Si film (corresponding to point 0 in Figure 1a) and after different lithiation stages (corresponding to point 1, 2, and 3 in Figure 1a). The different zones: SEI layer zone, Si thin film electrode zone (Si film) and current collector zone (SS substrate) with their interfaces are specified by horizontal arrows and the limits of these zones are marked by vertical dashed black lines in Figures 3 and 4. The first obvious phenomenon observed from ToF-SIM in-depth ion profiles is an increase in lithium content inside the Si thin film electrode, evidenced by a visible increase in the Li ion signal intensity as a function of the lithiation stage. This higher Li concentration is related to accumulation of Li-containing species in the near surface area because of SEI layer formation and also due to formation of Si−Li alloy compounds in the electrode bulk. The second evident phenomenon is an increase in sputtering time (necessary to reach the SS substrate interface) with propagation of lithiation reaction. This significantly higher sputtering time

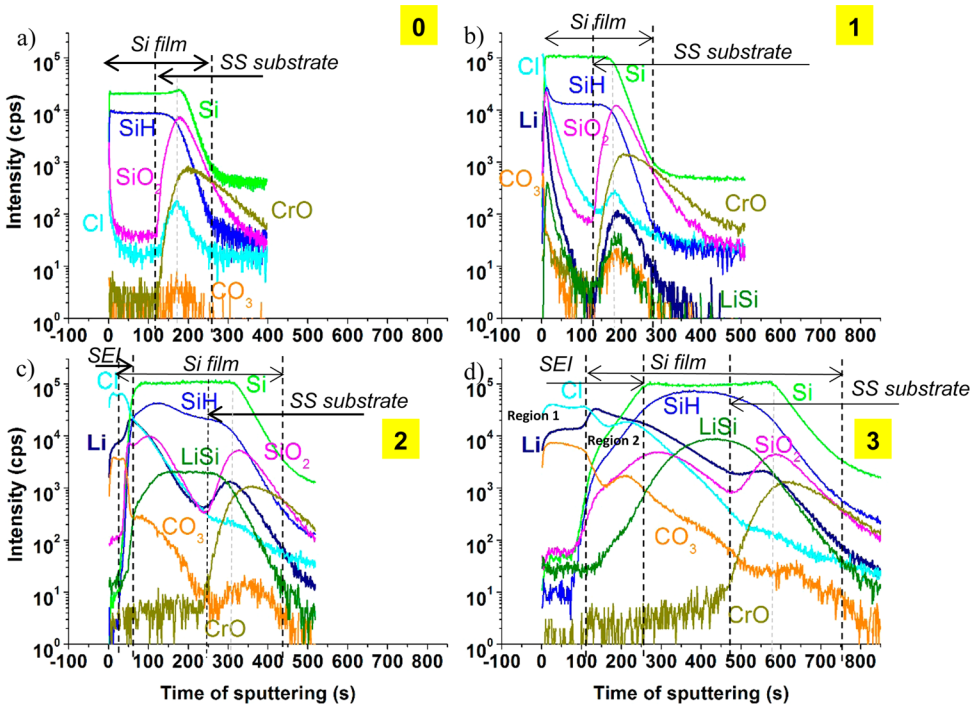

Figure 3. ToF-SIMS profiles of 100 nm Si thin film electrode as a function of lithiation stage: (a) at OCP (point 0), (b) 200 mV (point 1), (c) 200 mV half-lithiation plateau (point 2), and (d) 125 mV (point 3).

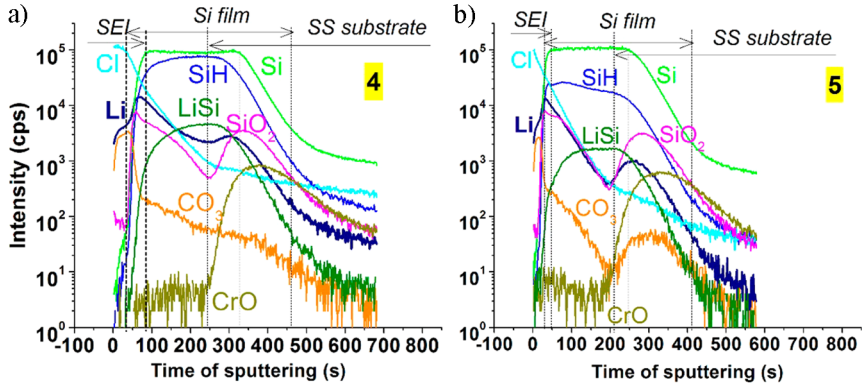

Figure 4. ToF-SIMS profiles of 100 nm Si thin film electrode as a function of delithiation stage: (a) 500 (point 4) and (b) 800 mV (point 5).

observed at each step of lithiation is directly related to a larger global volume of the Si film electrode. The width of the Si thin film electrode was determined from the interception point between SiO_2^- and CrO^- signals and it includes the Si electrode/SS substrate interfacial region (Figure 3). Volume modifications can be also evidenced by the increase in interfacial zones (longer sputtering time of SEI/Si electrode and Si electrode/SS substrate interface) and much less resolved in-depth ion profile shapes. The huge volume expansion/contraction can lead to a roughness increase in the thin film electrodes which is evidenced by enlarged interfacial zones. These types of modifications were already observed on other kinds of thin film electrodes.[21−23] In consequence, the roughness increase can lead to the exposure of a new uncovered Si electrode surface to the electrolyte. The other phenomena are related to the modification of surface composition (formation of the SEI layer) and lithiation process (formation of Li−Si alloys). The exact chemical composition of the surface layer was presented in details in our previous works.[7,8] These surface and bulk modifications can be easily identified on the basis of Si^- profiles. The time required to reach the plateau of Si^- signal increases with lithiation potential from almost 0 s for the pristine sample to around 250 s of sputtering for the lithiated sample (point 3) which indicates, first, the formation and, then, the uptake of SEI layer. The length of the Si plateau (the end of the Si^- plateau marked by a vertical dashed gray line in Figures 3 and 4) also increases with increasing the lithiation from 180 to 320 s for the pristine and completely lithiated samples, respectively, which is directly related to Li−Si alloying process responsible for film expansion (as presented in Figure 3d). Moreover, changes observed in Si^- profiles are also accompanied by different shapes of SiH^- and SiO_2^- profiles which are characteristic of Si film. A slight increase in the global SiH^- signal intensity can be observed after the first lithiation state (point 1, Figure 3b). The increase in SiH^- intensity close to the surface can be also noticed for the second lithiation point (point 2, Figure 3c). The shape of the SiO_2^- signal, characteristic of SiO_2 present on the Si film

dx.doi.org/10.1021/am502913q | ACS Appl. Mater. Interfaces 2014, 6, 13023−13033

surface (Figure 3a), is greatly influenced by lithium diffusion into Si bulk. In the first seconds of sputtering, there is a progressive enlargement (i.e., increase sputtering time) of the SiO_2^- signal for the first stage of lithiation (point 1, Figure 3b) and, then, during the next stage of lithiation the signal enlargement is accompanied by a decrease in the SiO_2^- signal intensity (Figure 3c and d). In the bulk Si-thin film electrode the intensity increase of the SiO_2^- signal can be observed, especially for the next stages of lithiation (Figure 3c and d). The electrolyte ($PC/LiClO_4$) and products of electrolyte decomposition can be a new source of oxygen species and lead to Si chemical oxidation. At the moment, this phenomenon is not completely understood and more studies need to be performed regarding the presence of SiO_2 species. However, the presence of silicon oxide (high intensity SiO_2^- profile) at the Si/SS substrate interface in the pristine sample originates from process of surface treatment by hydrogen before the thin film deposition by PECVD. Surface pretreatment with hydrogen should remove the native oxide layer from SS substrate, but ToF-SIMS profile shows formation of silicon oxide in the first stages of deposition in this Si/SS interfacial region.

Concerning the other ion profiles, in the first stages of reduction process (point 1, Figure 1a), before silicon lithiation plateau, new and intense signals, like Cl^-, CO_3^-, and Li^- appear (Figure 3b). They are characteristic of the SEI layer formation at the Si electrode surface. Before the silicon lithiation plateau (before point 1 Figure 1), the intensity of the $LiSi^-$ signal is low indicating that at this point no Li−Si alloys are formed confirming the occurrence of surface reactions. As the lithiation potential decreases, a progressive increase in the sputtering time can be observed for Cl^-, CO_3^- and Li^- signals (as shown in Figure 3c and 3d), which confirms the growth of the SEI layer. Moreover, ToF-SIMS profiles show 2 plateau domains in the SEI layer region (particularly visible in Figures 3c and d). This was first reported for amorphous Si thin film electrode cycled in $PC/LiClO_4$.[8] The first plateau region (marked as region 1 in Figure 3d) is characterized by very high Li^-, Cl^-, and CO_3^- and low Si^-, SiH^-, and SiO_2^- intensity signals. This indicates the formation of a distinct phase constituted of salt and carbonate reduction species characteristic of the SEI layer. Next, there is a transition region (between regions 1 and 2), which is characterized by a sudden decrease in the intensity of the Cl^- and CO_3^- signals and a simultaneous slight increase in the Li^- signal and a huge increase in the Si^-, SiH^-, and SiO_2^- signals intensities. A second plateau region with stable intensity values for Cl^- and CO_3^- signals is observed (region 2 in Figure 3d). This second region is also characterized by a continuous increase in the intensity of the Si^-, SiH^-, and SiO_2^- signals, characteristic of the Si film. The second region (marked as an interfacial region of the SEI/Si region 2 in Figure 3d) is poorly defined, since the signals corresponding to the SEI layer and the Si electrode are both detected. This second region is most probably due to expansion and increased roughness of the thin film silicon electrode during lithium alloying where signals attributed to both the Si electrode and the SEI layer can be collected. This kind of two-stage plateau was also characteristic for other types of thin film electrodes[20] and identified as the formation of duplex-like structure of the SEI layer.

The next region (marked as Si film) can be characterized by a stable intensity of Si^- and SiH^- signals, where a sharp decrease in the Cl^- and CO_3^- signals is visible. Moreover, an intense and rather stable $LiSi^-$ signal is collected in the bulk region of the Si film. This confirms the formation of Li−Si alloys in the Si film, which is in agreement with the galvanostatic test showing that the lithiation plateau region was reached (point 3 in Figure 1a).

To analyze the presence of defects (i.e., pinholes) in the Si thin film electrode, the CrO^- signal characteristic of stainless steel substrate was reported. A very low intensity of the CrO^- signal in the first seconds of acquisition reflects a defect-free Si thin film electrode. Formation of the SEI layer at the first state of lithiation (point 1, Figure 3b) leads to a slight increase in the CrO^- signal intensity in the first 10−20 s of sputtering, which indicates the formation of defects pinholes or cracks in the Si thin film electrode. This confirms (as mentioned above) the participation of the current collector (SS substrate) in surface reactions such as formation of the SEI layer. However, film expansion because of the formation of Li−Si alloy and growth of the SEI layer (points 2 and 3) leads to a drop of the CrO^- signal to a value near or lower than the one collected in pristine films (Figure 3c and d). This can be indicative of the formation of compact SEI layer on the electrode surface which results in good pinholes sealing.

From ToF-SIMS profiles, given in Figure 3a−d, one can infer a volume expansion and a continuous growth in the SEI layer with the increase in the lithiation potential. The volume expansion of the electrode reveals new parts of the Si thin film electrode where the electrolyte can be reduced. Electrolyte diffusion can be also facilitated by the formation of a rough and at the same time a more porous SEI layer structure or a high electronic conduction within the SEI layer.

Figure 4 shows ToF-SIMS depth profiles of Si films delithiated at 500 and 800 mV (point 4 and 5, respectively in Figure 1a) after cell relaxation to a stable OCP value. A decrease in the sputtering time for Cl^-, CO_3^-, and Li^- signals (corresponding to the components of the SEI layer) with an increase in the cutoff voltage can be observed (comparison of Figure 4a with b). This indicates that the SEI layer is unstable during the anodic process of delithiation and tends to dissolve. This confirms some recent FTIR results.[24] The same dynamic behavior of the SEI layer has been already observed on other types of negative electrodes.[22] At the same time, a decrease in the $LiSi^-$ signal intensity corresponds to the delithiation of a-Li_xSi:H. However, at 800 mV (point 5) some of the Li ions are still present in the silicon structure as Li_xSi alloy, which can be deduced from the high intensity of the $LiSi^-$ signal (Figure 4b). This means that the irreversible capacity value observed in the first cycle is not only due to the SEI layer formation but also to an incomplete delithiation of a-Li_xSi. The delithiation process leads also to a decrease in the sputtering time associated with shorter Si^- (to 210 s at delithiation state, point 5, in comparison to 320 s for lithiated sample, point 3) and SiH^- signal plateaus, which is in agreement with Si film contraction.

The Si volume variation can be calculated from the difference between Si final and Si initial volume at different points of lithiation or delithiation. More precisely, the volume changes in the Si electrode produced during the lithiation/delithiation process may be indirectly inferred from sputtering times of Si and SEI regions. Sputtering time variations of the Si + SEI (Δt_{Si+SEI}), Si (Δt_{Si}), and SEI layer (Δt_{SEI}) were calculated using the following equations, respectively:

$$\Delta t_{Si+SEI} = \frac{t_{Simeasured} - t_{Sipristine}}{t_{Sipristine}} \times 100\% \quad (1)$$

$$\Delta t_{Si} = \frac{(t_{Simeasured} - t_{SEI}) - t_{Sipristine}}{t_{Sipristine}} \times 100\% \quad (2)$$

$$\Delta t_{SEI} = \Delta t_{Si+SEI} - \Delta t_{Si} \quad (3)$$

The Δt_{Si+SEI}, Δt_{Si}, and Δt_{SEI} values were plotted as a function of the applied potential (200, 125, 500, 800 mV, corresponding to points 2, 3, 4, 5, respectively), as shown in Figure 5. As

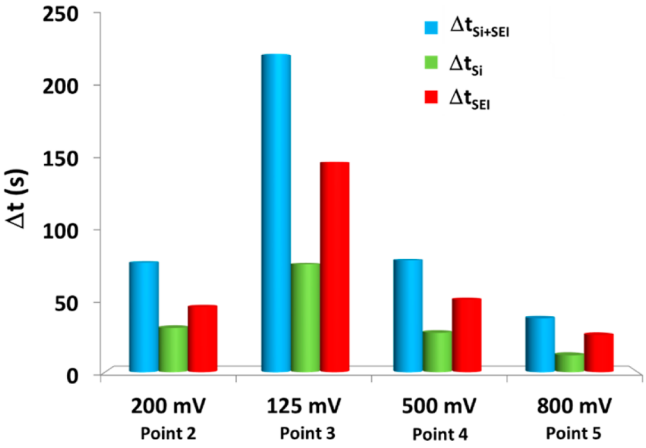

Figure 5. Sputtering time variation Δt (s) of Si + SEI (i.e., Si/SS interface position), Si, and SEI layer as a function of lithiation (point 2, 3) and delithiation (point 4, 5) stage.

already discussed above, these values increase with lithiation (point 2 and 3) and decrease with delithiation (point 4 and 5) processes. To evaluate silicon and SEI layer contribution to the total volume variation (given by the Δt_{Si+SEI} values), the Δt_{Si} and Δt_{SEI} values were compared with Δt_{Si+SEI} value. Histograms in Figure 5 show that Δt_{Si} represents only 1/3 of the total volume variation, while Δt_{SEI} contributes to 2/3 of the total volume variation. It can be then concluded from these results that the SEI layer contributes significantly to the volume modifications observed onto Si thin film electrodes. To our knowledge, these results evidencing the important contribution of electrolyte decomposition products (SEI layer) in the volume expansion of Si electrode derived from ToF-SIMS depth profiling data are shown here for the first time. Surface chemistry related to the electrolyte reactivity with the active electrode material seems to be an essential factor influencing both chemical and morphological modifications and, consequently, the electrochemical performance of Si electrodes.

3.2.2. Li Trapping as a Function of Electrode Film Thickness. In the aforementioned discussion, it was already concluded that Li accumulation can be easily observed in the near-surface zone corresponding to the SEI layer and in the Si film/SS substrate interface. This lithium interfacial trapping, particularly significant at the first point of lithiation (Figure 3 b), may explain OCP instability during the sample relaxation, as discussed above (and present in Figure 1). To investigate more carefully the phenomenon of lithium-ion trapping in Si electrode, the Li^- ion profiles were compared and analyzed for two different electrode thicknesses (30 and 100 nm) after full cycle of lithiation-delithiation at potential cutoff ~2 V (Figure 6). As the sputtering time depends on electrode thickness, and to be able to compare the intensities of Li^- profiles for these two films, the signals were normalized by multiplying the sputtering time of 30 nm Si film by

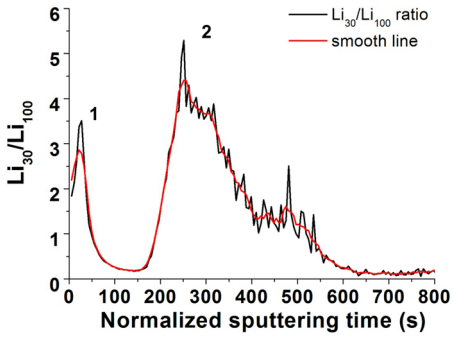

Figure 6. Li_{30}/Li_{100} ratio as a function of sputtering time in 30 and 100 nm Si thin film electrodes after a full cycle of lithiation/delithiation analyzed at a delithiated stage at potential cutoff ~2 V.

approximately 100/30 ratio, that is, the value of 3.33(3). Matrix effects on the sputtering rate for both films can be neglected. The ratio of lithium profiles for both electrodes (30 and 100 nm) Li_{30}/Li_{100} plotted against sputtering time shows two very intense Li^- "peak signals" (peaks 1 and 2 in Figure 6). The first peak, present between 0 and 50 s of sputtering, corresponds to lithium and species containing lithium ions accumulated in the SEI layer formed on the surface of the Si electrode. The second peak, present between 200 and 300 s of sputtering, corresponds to an accumulation of lithium at the Si electrode/SS substrate interface. Very low lithium signal can be observed in the bulk of both electrodes (between ~100−170 s of sputtering given in normalized plot of Figure 6). This result shows that Li trapping occurs mainly at the interfaces, regardless of the Si film thickness. However, a higher absolute intensity of Li^- signal ($Li_{30}/Li_{100} \gg 1$) indicates an easier trapping of Li ions in thinner films, which confirms the conclusions presented above concerning the high reactivity at the Si electrode/SS substrate interface. These findings are consistent with the higher capacity loss observed in the thinner Si films as observed by the electrochemical results (Figure 2b). On the basis of these results, it can be concluded that by decreasing Si dimensions (i.e., thickness of thin film electrode or dimensions of nanostructured architectures), lithium trapping becomes a critical parameter. Lithium trapping, described in the literature as lithium segregation in Si and at interfaces[5,17,25−27] can significantly influence electrochemical performances of the Si electrode. These results show that electrode architecture is also one of the primordial parameters, which should be taken into account for improving electrochemical performances of Si electrodes and thus the LIB cells.

3.2.3. Effect of Cycling on Chemical and Morphological Modifications. Figure 7a shows ToF-SIMS depth profiles of 30 nm Si pristine and cycled films (52 and 100 cycles) performed in PC/$LiClO_4$, between 125 mV and 2 V vs Li/Li^+. A significant evolution of the Li^-, Si^-, and CrO^- signals characteristic of the SEI layer, Si film and SS current collector, respectively, can be observed as a function of cycling. The first evident evolution is an increase in the sputtering time for all the signals and the loss of sharpness of interfaces between the SEI layer/Si film and also the Si film/SS substrate. This is particularly illustrated by the lack of definition of the interfaces for the Si^- signal with increasing number of cycles (Figure 7a after 100 cycles). These modifications are related to strong changes of the chemistry and morphology (volume expansion and roughness increase) of the Si film electrode. As discussed above, the SEI layer is unstable during the lithiation/delithiation process (see Figures

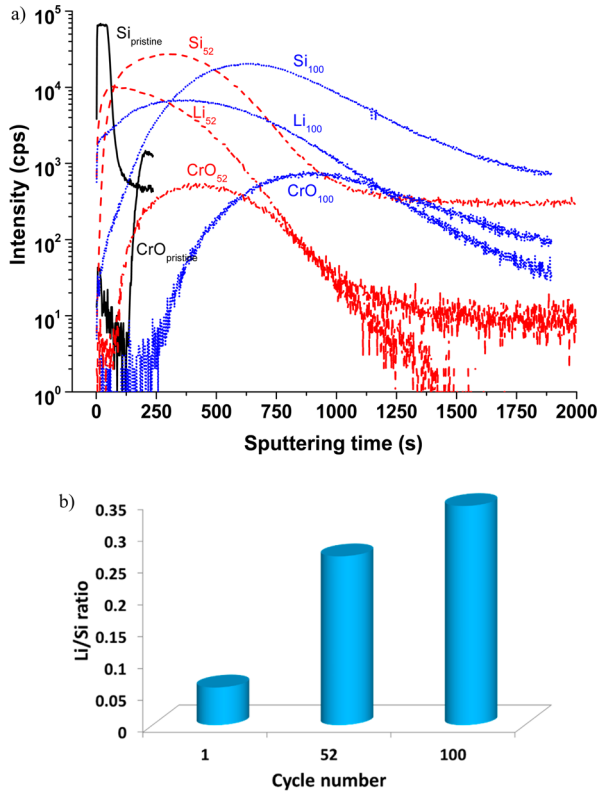

Figure 7. (a) ToF-SIMS depth profiles of 30 nm Si pristine and cycled films (52 and 100 cycles) performed in PC/$LiClO_4$, between 125 mV and 2 V vs Li/Li^+; (b) Li/Si ratio evolution of Si films with cycling.

3a–d and 4a and b). A thick SEI layer is formed during lithiation and undergoes dissolution during delithiation process. Here, the instability of the SEI layer and its continuous uptake as a function of cycling can be confirmed by a longer time necessary to attain the maximum intensity of the Si^- profile (280 s for 52 cycles and 600 s for 100 cycles). A similar dynamic behavior of the SEI layer upon cycling on negative electrodes has been previously described.[22] For graphite electrodes Edström et al.[28] suggested a microporous structure of the SEI layer, while Tasaki[29] emphasized that a dynamic behavior of the SEI layer means the modification of the SEI chemical composition induced by the electrolyte composition. Formation of a rough and microporous-like structure of the SEI layer on the Si electrodes cannot be excluded. This could be explained by less resolved depth profile shapes.

Retention or trapping of some products of electrolyte decomposition, formed during reduction, can explain the irreversible volume expansion observed in Si film after 100 cycles, which can be deduced from high sputtering times (Figure 7a). Despite huge and irreversible chemical and morphological changes in Si films, a relatively good capacity retention can be observed (as shown and discussed above, see Figure 2a) and mobility of lithium ions remains possible in deeply deteriorated material. This can be due to higher porosity of the material with cycling and/or to the SEI layer conducting properties. Figure 7b shows Li/Si ratio evolution of Si films with cycling. As the number of cycles increases the quantity of Li retained in the Si increases, confirming once more the phenomenon of lithium trapping.

3.3. Chemical Diffusion Coefficient of Li Ions in Si Thin Film Electrode. ToF-SIMS allows direct measurements of lithium concentration and has been recently applied to study transport in the SEI layer[30,31] and a partially delithiated olivine-type $LiFePO_4$ cathode.[32]

The apparent diffusion coefficient of lithium (D_{Li}) in the Si film electrode can be directly obtained from Li-ion in-depth profile obtained by ToF-SIMS measurement (presented in Figure 8a) and then calculated from the semi-infinite

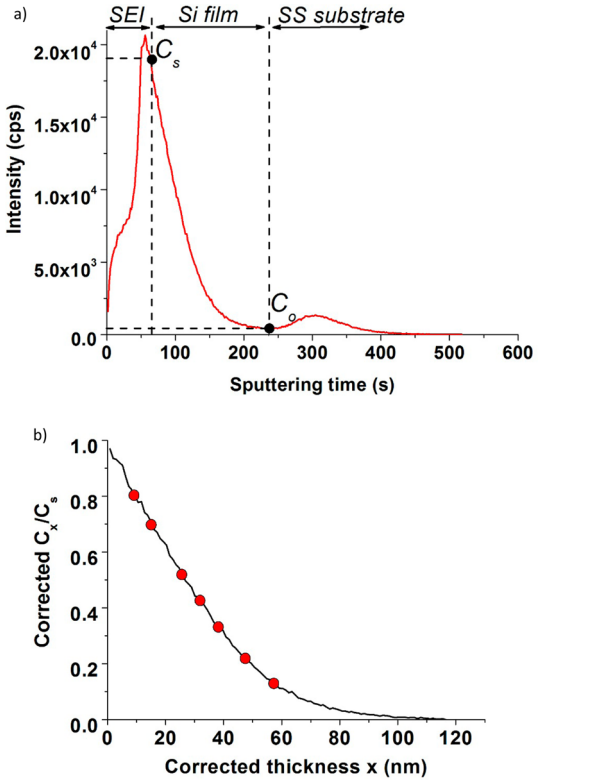

Figure 8. (a) Li ion ToF-SIMS depth profile at 200 mV (half-plateau lithiation). (b) Plot of C_s/C_x as a function of Si film depth (x).

integration of Fick's second law for one-dimensional diffusion:[33,34]

$$\frac{\partial C}{\partial t} = \frac{\partial}{\partial x}\left(D_{Li}\frac{\partial C}{\partial x}\right) = D_{Li}\frac{\partial^2 C}{\partial x^2} \quad (4)$$

where C is the concentration of lithium in the bulk electrode at depth x and after time t. The following assumptions have been taken into account: (a) lithium concentration in the electrolyte is high enough to supply Li-ion during the whole lithiation process (alloying); (b) a constant field force is applied in the plateau region (stable potential around 200 mV); and (c) the SEI layer region (around the first 60 s of sputtering) is excluded (see Figure 8a).

The solution of eq 4 is a concentration profile as a function of time $C(x,t)$. Hence, Fick's second law describes lithium ion accumulation in the material with time, that is, changes in concentration profile and concentration gradient with time. Lithium ion diffusion coefficient (D_{Li}) is considered to be independent of x and C. The analytical solution of Fick's second law, for short times, is given by Gaussian error function:

$$\mathrm{erf}(y) = \frac{2}{\sqrt{\pi}}\int_0^y \exp(-y^2)\cdot\partial y \quad (5)$$

by setting boundary conditions.

dx.doi.org/10.1021/am502913q | ACS Appl. Mater. Interfaces 2014, 6, 13023–13033

If we consider eq 4, D as a constant and we use the function $y = f(x,t)$ defined by

$$y = \frac{x}{2\sqrt{Dt}} \tag{6}$$

The partial derivatives of eq 6 are

$$\frac{\partial y}{\partial x} = \frac{1}{2\sqrt{Dt}} \text{ and } \frac{\partial y}{\partial t} = -\frac{x}{4\sqrt{Dt^3}} \tag{6a}$$

By definition

$$\frac{\partial C}{\partial t} = \frac{\partial C}{\partial y}\frac{\partial y}{\partial t} = -\frac{x}{4\sqrt{Dt^3}}\frac{\partial C}{\partial y} \tag{6b}$$

and

$$\frac{\partial^2 C}{\partial x^2} = \frac{\partial}{\partial y}\left[\frac{\partial C}{\partial y}\left(\frac{\partial y}{\partial x}\right)\right] = \frac{1}{4Dt}\frac{\partial^2 C}{\partial y^2} \tag{6c}$$

When substituting eqs 6b and 6c into eq 4, we obtain

$$\frac{\partial C}{\partial y} = -\frac{\sqrt{Dt}}{x}\frac{\partial^2 C}{\partial y^2} \tag{7}$$

Combining eqs 6 and 7, we obtain the following equation:

$$\frac{\partial C}{\partial y} = -\frac{1}{2y}\frac{\partial^2 C}{\partial y^2} \tag{8}$$

Now if $z = (\partial C)/(\partial y)$ the eq (8) is simplified to

$$z = -\frac{1}{2y}\frac{dz}{dy} \tag{8a}$$

It then can be rearranged into

$$-2\int y\partial y = \int \frac{\partial z}{z} \tag{8b}$$

By integration

$$-y^2 = \ln z - \ln B \tag{8c}$$

where B is an integration constant.

Rearranging eq 8c gives

$$z = B\exp(-y^2) \tag{9}$$

And

$$\int dC = B\int \exp(-y^2)dy \tag{10}$$

To solve this integral, a set of boundary conditions are necessary, as given below

$$C = \begin{cases} C_x = C_s \quad \text{for} \quad y = 0 \text{ at } t > 0 \text{ and } x = 0, \text{ where } C_s \\ \qquad\qquad\qquad \text{is surface [Li ion] concentration} \\ C_x = C_0 \quad \text{for} \quad y = \infty \text{ at } t = 0 \text{ and } x > 0, \text{ where } C_0 \\ \qquad\qquad\qquad \text{is bulk [Li ion] concentration} \end{cases}$$

$$\int_{C_s}^{C_0} dC = B\int_0^{\infty} \exp(-y^2)\, dy \tag{11}$$

$$C_0 - C_s = B\frac{\sqrt{\pi}}{2} \tag{11a}$$

$$B = \frac{2}{\sqrt{\pi}}(C_0 - C_s) \tag{11b}$$

When bulk concentration ($C_0 = C_x$ at $x = \infty$) becomes greater than surface concentration ($C_s = C_x$ at $x = 0$) the solution of Fick's second law (eq 4) for concentration polarization ($C_0 > C_s$) becomes

$$\int_{C_0}^{C_x} dC = B\int_{\infty}^{y} \exp(-y^2)\, dy = -B\int_{y}^{\infty} \exp(-y^2)\, dy \tag{12}$$

$$C_x - C_s = -\frac{2}{\sqrt{\pi}}(C_0 - C_s)\frac{\sqrt{\pi}}{2}\text{erfc}(y) \tag{12a}$$

$$\frac{C_x - C_0}{C_s - C_0} = 1 - \text{erf}\left(\frac{x}{2\sqrt{Dt}}\right) \text{ for } C_0 > C_s \tag{12b}$$

This equation can be presented as

$$\frac{C_x - C_0}{C_s - C_0} = 1 - \text{erf}(z) \text{ with } z = \frac{x}{2\sqrt{Dt}} \tag{12c}$$

For $C_0 \approx 0$ equation can be simplified to

$$\frac{C_x}{C_s} = 1 - \text{erf}(z) \tag{12d}$$

Figure 8a displays the Li ion ToF-SIMS profile (on a linear scale) collected at point 2 (at half lithiation plateau, Figure 1a). The decay of Li ion concentration as a function of sputtering time shows that Si film has been only partially lithiated (Figure 8a). The linear decrease of the lithium concentration as a function of sputtering time (thickness of Si thin film electrode) can be explained by the fact that this ToF-SIMS profile was performed on the sample lithiated with fast cycling rate. C_s and C_0 values displayed in Figure 8a correspond to lithium concentration at the SEI/Si interface and up to Si/SS substrate interface (i.e., [Li] in the Si bulk), respectively. Then, the data were normalized with respect to background (corresponding to C_0 value) and to C_s value. The sputtering time was converted to Si film thickness, knowing that the sputtering rate is of ~0.6 nm/s. For simplicity, the modification of electrode matrix after lithiation (i.e., related to Li trapping), was neglected and the sputtering rate was obtained from ToF-SIMS depth profiles performed for different thicknesses of pristine Si thin film electrodes. Data were replotted again as C_x/C_s vs Si film's depth (x) (Figure 8b). From this curve, we were able to obtain erf(z) and, thereafter, to determine z value by iteration method from error function tables. D_{Li} value was estimated to be ~5.9 × 10^{-15} cm^2 s^{-1} in Si film after 1250 s of Si lithiation (Table 1). In Table 2, this measured value for D_{Li} is compared with data reported by other authors.[35−43] This low value shows that the ionic transport can be limited by trapping of Li ions in the SEI layer and in the bulk of electrode (most probably in the SiO_2/Si interface zones), as evidenced by ToF-SIMS results presented above. Yoshimura et al.[41] reported that D_{Li} value increased from 10^{-13} to 10^{-10} cm^2 s^{-1} as Si film thickness increased. However, D_{Li} should be independent of the thickness for Fick's second law to be applicable. This behavior was attributed to a surface limiting reaction process, since as the film thickness, increases surface reactions become less important. In our case, continuous growth of the SEI layer in the silicon lithiation domain (~200 mV) can explain rather low values of lithium diffusion in silicon. The ionic transport can be also hindered by

Table 1. C_x/C_s, erf(z), z, z^2, and x Values and Lithium Ion Diffusion Coefficient (D_{Li}) Calculated from $D_{Li} = (x^2)/(4z^2t)$ for t = 1250 s (Corresponding to Half-Plateau Lithiation Time Taken from Figure 1a)

C_x/C_s	x (10^{-7} cm^2)	erf(z)	z	z^2	x^2 (10^{-14} cm^2)	D_{Li} (10^{-15} cm^2 s^{-1})
0.8010	9.49	0.1990	0.1892	0.0358	90.1	5.0335
0.7095	14.9	0.2905	0.2635	0.0694	222	6.3976
0.4975	26.8	0.5025	0.4800	0.2304	718	6.2326
0.3920	34.4	0.6098	0.6077	0.3693	1183	6.4067
0.3196	39.7	0.6804	0.7039	0.4955	1576	5.9576
0.2004	49.5	0.7996	0.9056	0.8201	2450	5.9748
0.1000	63.5	0.9000	1.1657	1.3588	4032	5.9346
0.0509	73.3	0.9491	1.3826	1.9116	5372	5.6204

Table 2. Comparison of the Measured Lithium Ion Diffusion Coefficient (D_{Li}) with Data Reported in the Literature for Silicon

silicon	technique	D_{Li} (cm^2 s^{-1})	ref
a-Si:H (PECVD)	Tof-SIMS depth profiling	6×10^{-15}	this work
nano-Si	CV, PITT, GITT, and EIS	10^{-12}	35
a-Si:H (CVD)	CV	10^{-13}	36, 37
a-Si:H (CVD)	EIS	10^{-13}	38
a-Si (RF magnetron sputtering)	PITT and EIS	10^{-12}–10^{-13}	39
Si vacuum-deposited films	EIS, PITT	10^{-11}–10^{-13}	40, 41
a-Si pulsed laser deposition (PLD)	CV	10^{-13}	42
a-Si vacuum-deposited film	bipolar cells	10^{-9}	43
c-Si plate (180 μm)	bipolar cells	10^{-11}	43

[a] D_{Li} increases from 10^{-13} to 10^{-10} cm^2 s^{-1} as film thickness increases. Potential has a very low impact on D_{Li} values.

other phenomena like formation of SiO_2 species due to contact of silicon with electrolyte. The SiO_2 species tend to increase in the bulk of the silicon electrode with cycling. In this case lithium could be trapped in the surface of Si particles probably as Li_4SiO_4[17] and also limit Li^+ diffusion.

This simple approach of evaluation of Li diffusion by application of ToF-SIMS depth profiling has few drawbacks and much attention should be paid in order to obtain reliable information. These weak points are related to (a) Li ion profile, which can provide information on lithium distribution at the same time in the SEI layer, Li_xSi alloys and $Li_xSi_yO_z$; (b) morphological modifications (material expansion, roughness increase) of thin film electrode material at lithiated state (corresponding to half-plateau potential) for which the ToF-SIMS depth profiles show poor defined interfaces (where a discrimination of different zones like SEI layer contribution can be difficult); film expansion during lithiation leads to continuous change in Li^+ travel depths and thereafter Li^+ concentration; and (c) interfacial lithium trapping which can change Li^+ conduction mechanisms by blocking preferential paths and then influence Li concentration in Si film leading to different D_{Li} values. In this way, Li trapping and Si expansion contribute most probably to both Li concentration profile change and D_{Li} variation with depths of lithiation.

At the same time, the Li-ion in-depth profile obtained by ToF-SIMS which is a direct measurement method of the apparent diffusion coefficient, gives a thorough insight on lithium distribution into the electrode material and this methodology can be applied to any type of electrode material. It must be emphasized that this method is the first approach of ToF-SIMS application in the studies of kinetics concerning the lithium transport in thin film electrode materials.

4. CONCLUSIONS

This work studies has shown that the electrochemical reaction of lithium within Si thin film negative electrode materials induced significant chemical and morphological modifications. The in-depth profiles measured by ToF-SIMS is a unique tool, which has revealed these modifications at different stages of lithiation/delithiation and number of cycles. The major findings are the following: (1) Instability of the SEI layer during the first cycle and SEI layer uptake during lithiation and dissolution during delithiation, (2) significant SEI layer growth upon cycling, (3) irreversible Si thin film electrode swelling/deswelling process during the lithiation/delithiation, (4) continuous expansion and or pulverisation of the Si electrode with cycling, (5) an important contribution, as far as 60%, of the SEI layer in the total volume variation of Si electrode, (6) lithium and other ions (related to products of electrolyte decomposition) trapping and segregation at interfaces with increasing number of cycles, and (7) relatively low apparent Li ion diffusion coefficient value obtained from ToF-SIMS Li-ion depth profiling, of order of $\sim 5.9 \times 10^{-15}$ cm^2 s^{-1} in Si thin film electrode, which can be entailed by Li trapped in the bulk of electrode material (most probably at Si/SiO_2 interfaces) or the SEI layer.

The electrode modifications listed above are detrimental to the cycling stability of silicon electrodes. This application of ToF-SIMS Li-ion depth profiling applied for calculation of Li diffusion in Si thin film electrode material is the first approach and even of some drawbacks of this method, it gives a thorough insight on lithium distribution into the electrode material and can be applied to any type of electrode material.

AUTHOR INFORMATION

Corresponding Author

*Tel: +33(0)144278026. E-mail: jolanta.swiatowska@chimie-paristech.fr.

Notes

The authors declare no competing financial interest.

ACKNOWLEDGMENTS

The authors would like to acknowledge Renault and Institut de la Mobilité Durable (IMD) for financial support of this work, as well as Région Ile-de-France for partial funding of the ToF-SIMS equipment.

REFERENCES

(1) Green, M.; Fielder, E.; Scrosati, B.; Wachtler, M.; Moreno, J. S. Structured Silicon Anodes for Lithium Battery Applications. *Electrochem. Solid-State Lett.* **2003**, *6*, A75–A79.

(2) Nanda, J.; Datta, M. K.; Remillard, J. T.; O'Neill, A.; Kumta, P. N. In Situ Raman Microscopy During Discharge of a High Capacity Silicon–Carbon Composite Li-Ion Battery Negative Electrode. *Electrochem. Commun.* **2009**, *11*, 235–237.

(3) Limthongkul, P.; Jang, Y.-I.; Dudney, N. J.; Chiang, Y.-M. Electrochemically-Driven Solid-State Amorphization in Lithium–Metal Anodes. *J. Power Sources* **2003**, *119*, 604–609.

(4) Pal, S.; Damle, S. D.; Kumta, P. N.; Maiti, S. Modeling of Lithium Segregation Induced Delamination of a-Si Thin Film Anode in Li-Ion Batteries. *Comput. Mater. Sci.* **2013**, *79*, 877−887.
(5) Stournara, M. E.; Xiao, X.; Qi, Y.; Johari, P.; Lu, P.; Sheldon, B. W.; Gao, H.; Shenoy, V. B. Li Segregation Induces Structure and Strength Changes at the Amorphous Si/Cu Interface. *Nano Lett.* **2013**, *13*, 4759−4768.
(6) Hao, F.; Fang, D. Reducing Diffusion-Induced Stresses of Electrode-Collector Bilayer in Lithium-Ion Battery by Pre-Strain. *J. Power Sources* **2013**, *242*, 415−420.
(7) Pereira-Nabais, C.; Swiatowska, J.; Chagnes, A.; Gohier, A.; Zanna, S.; Seyeux, A.; Tran-Van, P.; Cojocaru, C.-S.; Cassir, M.; Marcus, P. Insigth on the Solid Electrolyte Interphase (SEI) onto Si Nanowires in Lithium-Ion Battery: Chemical and Morphological Modifications Upon Cycling. *J. Phys. Chem. C* **2014**, *118*, 2919−2928.
(8) Pereira-Nabais, C.; Swiatowska, J.; Chagnes, A.; Ozanam, F.; Gohier, A.; Tran-Van, P.; Cojocaru, C.-S.; Cassir, M.; Marcus, P. Interphase Chemistry of Si Electrodes Used as Anodes in Li-Ion Batteries. *Appl. Surf. Sci.* **2013**, *266*, 5−16.
(9) Philippe, B.; Dedryvère, R.; Gorgoi, M.; Rensmo, H.; Gonbeau, D.; Edstrom, K. Role of the $LiPF_6$ Salt For The Long-Term Stability of Silicon Electrodes In Li-Ion Batteries—A Photoelectron Spectroscopy Study. *Chem. Mater.* **2013**, *25*, 394−404.
(10) Nakai, H.; Kubota, T.; Kita, A.; Kawashima, A. Investigation of the Solid Electrolyte Interphase Formed by Fluoroethylene Carbonate on Si Electrodes. *J. Electrochem. Soc.* **2011**, *158*, A798−A801.
(11) Choi, N.-S.; Yew, K. H.; Kim, H.; Kim, S.-S.; Choi, W.-U. Surface Layer Formed on Silicon Thin-Film Electrode Lithium Bis(oxalate) Borate-Based Electrolyte. *J. Power Sources* **2007**, *172*, 404−409.
(12) Martin, L.; Martinez, H.; Ulldemolins, M.; Pecquenard, B.; Le Cras, F. Evolution of the Si Electrode/Electrolyte Interface in Lithium Batteries Characterized by XPS and AFM Techniques: The Influence of Vinylene Carbonate Additive. *Solid State Ionics* **2012**, *215*, 36−44.
(13) Choi, N.-S.; Yew, K. H.; Lee, K. Y.; Sung, M.; Kim, H.; Kim, S.-S. Effect of Fluoroethylene Carbonate Additive on Interfacial Properties of Silicon Thin-Film Electrode. *J. Power Sources* **2006**, *161*, 1254−1259.
(14) Chen, L.; Wang, K.; Xie, X.; Xie, J. Effect Of Vinylene Carbonate (VC) As Electrolyte Additive on Electrochemical Performance of Si Film Anode For Lithium Ion Batteries. *J. Power Sources* **2007**, *174*, 538−543.
(15) Etacheri, V.; Haik, O.; Goffer, Y.; Roberts, G. A.; Stefan, I. C.; Fasching, R.; Aurbach, D. Effect of Fluoroethylene Carbonate (FEC) on the Performance and Surface Chemistry of Si-Nanowire Li-Ion Battery Anodes. *Langmuir* **2012**, *28*, 965−976.
(16) Chan, C. K.; Ruffo, R.; Hong, S. S.; Cui, Y. Surface Chemistry and Solid Electrolyte Interphase of Silicon Nanowire Anodes in Lithium-Ion Batteries. *J. Power Sources* **2009**, *189*, 1132−1140.
(17) Philippe, B.; Dedryvére, R.; Allouche, J.; Lindgren, F.; Gorgoi, M.; Rensmo, H.; Gonbeau, D.; Edström, K. Nanosilicon Electrodes for Lithium-Ion Batteries: Interfacial Mechanisms Studied by Hard and Soft X-ray Photoelectron Spectroscopy. *Chem. Mater.* **2012**, *24*, 1107−1115.
(18) Profatilova, I. A.; Choi, N.-S.; Yew, K. H.; Choi, W.-U. The Effect of Ethylene Carbonate on the Cycling Performance of a Si Electrode. *Solid State Ionics* **2008**, *179*, 2399−2405.
(19) Wen, Z.-S.; Ke, W.; Xie, J.-Y. Interface Formed on High Capacity Silicon Anode for Lithium Ion Batteries. *J. Inorg. Mater.* **2007**, *22*, 437−441.
(20) Li, J.-T.; Maurice, V.; Swiatowska-Mrowiecka, J.; Seyeux, A.; Zanna, S.; Klein, L.; Sun, S.-G.; Marcus, P. XPS, Time-of-Flight-SIMS and Polarization Modulation IRRAS Study of Cr_2O_3 Thin Film Materials as Anode for Lithium Ion Battery. *Electrochim. Acta* **2009**, *54*, 3700−3707.
(21) Tian, B.; Światowska, J.; Maurice, V.; Zanna, S.; Seyeux, A.; Klein, L. H.; Marcus, P. Combined Surface and Electrochemical Study of the Lithiation/Delithiation Mechanism of Iron Oxide Thin Film Anode for Lithium-Ion Batteries. *J. Phys. Chem. C* **2013**, *117*, 21651−21661.
(22) Liao, F.; Światowska, J.; Maurice, V.; Seyeux, A.; Klein, L. H.; Zanna, S.; Marcus, P. Electrochemical Lithiation and Passivation Mechanisms of Iron Monosulfide Thin Film as Negative Electrode Material for Lithium-Ion Batteries Studied by Surface Analytical Techniques. *Appl. Surf. Sci.* **2013**, *283*, 888−899.
(23) Liao, F.; Światowska, J.; Maurice, V.; Seyeux, A.; Klein, L. H.; Zanna, S.; Marcus, P. Ageing Mechanisms of Conversion-Type Electrode Material Studied on Iron Sulfide Thin Films. *Electrochim. Acta* **2014**, *120*, 359−368.
(24) Alves Dalla Corte, D. Effets du Traitement Chimique de la Surface d'une Electrode Négative en Silicium Amorphe pour Batterie Lithium-Ion: Etude par Spectroscopie Infrarouge In Situ. PhD Thesis, Ecole Polytechnique, October, 2013.
(25) Winer, K.; Street, R. A. Interstitial Li Doping of a-Si:H. *J. Appl. Phys.* **1989**, *65*, 2272.
(26) Delpuech, N.; Dupré, N.; Mazouzi, D.; Gaubicher, J.; Moreau, P.; Bridel, J. S.; Guyomard, D.; Lestriez, B. Correlation Between Irreversible Capacity and Electrolyte Solvents Degradation Probed by NMR in Si-Based Negative Electrode of Li-Ion Cell. *Electrochem. Commun.* **2013**, *33*, 72−75.
(27) Oumellal, Y.; Delpuech, N.; Mazouzi, D.; Dupré, N.; Gaubicher, J.; Moreau, P.; Soudan, P.; Lestriez, B.; Guyomard, D. The Failure Mechanism of Nano-Sized Si-Based Negative Electrodes for Lithium Ion Batteries. *J. Mater. Chem.* **2011**, *21*, 6201.
(28) Edström, K.; Herstedt, M.; Abraham, D. A New Look at the Solid Electrolyte Interphase on Graphite Anodes in Li-Ion Batteries. *J. Power Sources* **2006**, *153* (2), 380−384.
(29) Tasaki, K.; Goldberg, A.; Lian, J.-J.; Walker, M.; Timmons, A.; Harris, S. J. Solubility of Li Salts Formed on the Li Ion Battery Negative Electrode. *J. Electrochem. Soc.* **2009**, *156*, A1019.
(30) Lu, P.; Harris, S. J. Lithium Transport within the Solid Electrolyte Interphase. *Electrochem. Commun.* **2011**, *13*, 1035−1037.
(31) Shi, S.; Lu, P.; Liu, Z.; Qi, Y.; Hector, L. G.; Li, H.; Harris, S. J. Direct Calculation of Li-ion Transport in the Solid Electrolyte Interphase. *J. Am. Chem. Soc.* **2012**, *134*, 15476−15487.
(32) Weichert, K.; Sigle, W.; van Aken, P. A.; Jamnik, J.; Zhu, C.; Amin, R.; Acartürk, T.; Starke, U.; Maier, J. Phase Boundary Propagation in Large $LiFePO_4$ Single Crystals on Delithiation. *J. Am. Chem. Soc.* **2012**, *134*, 2988−2992.
(33) Crank, J. In *The Mathematics of Diffusion*; Oxford Univ. Press: Oxford, U.K., 2002; pp 28−39.
(34) Schwarzburger, N. I.; Knobel, R.; Behrens, H.; Binnewies, M.; Horn, I.; Pelster, A.; Arlinghaus, H. F.; Dörrer, L.; Schmidt, H. Kinetics of Lithium Intercalation in Titanium Disulfide Single Crystals. *Z. Phys. Chem.* **2012**, *226*, 461−489.
(35) Ding, N.; Xu, J.; Yao, Y. X.; Wegner, G.; Fang, X.; Chen, C. H.; Lieberwirth, I. Determination of the Diffusion Coefficient of Lithium Ions in Nano-Si. *Solid State Ionics* **2009**, *180*, 222−225.
(36) Kulova, T. L.; Skundin, A. M.; Pleskov, Y. V.; Terukov, E. I.; Kon'kov, O. I. Lithium Intercalation in Thin Amorphous-Silicon Films. *Russ. J. Electrochem.* **2006**, *42*, 363−369.
(37) Kulova, T. L.; Skundin, A. M.; Pleskov, Y. V.; Terukov, E. I.; Kon'kov, O. I. Lithium Insertion Into Amorphous Silicon Thin-Film Electrodes. *J. Electroanal. Chem.* **2007**, *600*, 217−225.
(38) Kulova, T. L.; Pleskov, Y. V.; Skundin, A. M.; Terukov, E. I.; Kon'kov, O. I. Lithium Intercalation Into Amorphous-Silicon Thin Films: An Electrochemical-Impedance Study. *Russ. J. Electrochem.* **2006**, *42*, 708−714.
(39) Xie, J.; Imanishi, N.; Zhang, T.; Hirano, A.; Takeda, Y.; Yamamoto, O. Li-Ion Diffusion in Amorphous Si Films Prepared by RF Magnetron Sputtering: A Comparison of Using Liquid and Polymer Electrolytes. *Mater. Chem. Phys.* **2010**, *120*, 421−425.
(40) Zhang, T.; Zhang, H. P.; Yang, L. C.; Wang, B.; Wu, Y. P.; Takamura, T. The Structural Evolution and Lithiation Behavior of Vacuum-Deposited Si film with High Reversible Capacity. *Electrochim. Acta* **2008**, *53*, 5660−5664.

(41) Yoshimura, K.; Suzuki, J.; Sekine, K.; Takamura, T. Evaluation of the Li Insertion/Extraction Reaction Rate at a Vacuum-Deposited Silicon Film Anode. *J. Power Sources* **2005**, *146*, 445.
(42) Xia, H.; Tang, S.; Lu, L. Properties of Amorphous Si Thin Film Anodes Prepared by Pulsed Laser Deposition. *Mater. Res. Bull.* **2007**, *42*, 1301−1309.
(43) Yoshimura, K.; Suzuki, J.; Sekine, K.; Takamura, T. Measurement of the Diffusion Rate of Li in Silicon by the Use of Bipolar Cells. *J. Power Sources* **2007**, *174*, 653−657.